Cell, Volume *136*

Supplemental Data

Topology and Regulation of the Human eIF4A/4G/4H Helicase Complex in Translation Initiation

Assen Marintchev, Katherine A. Edmonds, Boriana Marintcheva, Elthea Hendrickson, Monika Oberer, Chikako Suzuki, Barbara Herdy, Nahum Sonenberg, and Gerhard Wagner

Supplemental Results

Interactions of eIF4A with eIF4G HEAT-2

We studied the binding between the two domains of eIF4A and eIF4G HEAT-2 by NMR chemical shift perturbation assays. In this experiment one protein is labeled with stable isotopes (e.g., ^{15}N) and ^{1}H-^{15}N-HSQC (heteronuclear single-quantum coherence) spectra are collected in the presence and absence of the unlabeled ligand. In the ^{1}H-^{15}N-HSQC experiment, each peak corresponds to an NH group in the labeled protein and the peak position is at the intersection of the chemical shifts of the ^{1}H and ^{15}N nuclei. If an unlabeled ligand binds to the protein, it affects some of the NH groups in the labeled protein. The observed result is that a subset of the peaks in the spectrum "move". The regions of the labeled protein affected by the interaction can be mapped if the backbone NMR resonance assignments are available (if it is known which peak in the HSQC spectrum corresponds to which residue). No changes in the spectrum are observed if the unlabeled ligand fails to bind at the concentrations used.

Both eIF4A-NTD and eIF4A-CTD bound to eIF4G HEAT-2 (see **Figure 3AB** in the main text). The interaction between eIF4A-NTD and eIF4G HEAT-2 was in fast to

intermediate exchange regime on the NMR time scale. Use of TROSY (transverse relaxation-optimized spectroscopy) was necessary to observe the spectra of the 1:1 eIF4A-NTD:eIF4G HEAT-2 complex (**Figure 3A**), indicative of the formation of a large complex (~50 kDa). In contrast, binding of eIF4A-CTD to eIF4G HEAT-2 appeared weaker, in fast exchange and with much smaller chemical shift changes (**Figure 3B**). There was no severe line broadening in the ^{1}H-^{15}N-HSQC spectra of eIF4G HEAT-2 in the presence of equimolar amount of eIF4A-CTD, indicating that the ~45 kDa eIF4A-CTD:eIF4G HEAT-2 complex was formed only transiently and was in equilibrium with the free species, eIF4A-CTD (~20 kDa) and eIF4G HEAT-2 (~25 kDa).

The eIF4G HEAT-2 surfaces affected by eIF4A-NTD binding (colored navy in **Figure 3C**) were mostly around the loop between α-helices 5 and 6 and the adjacent loop between α-helices 3 and 4. Smaller chemical shift changes were observed along the interfaces of the third helical hairpin (α-helices 5, 6) with the second and fourth helical hairpins (α-helices 3, 4 and 7, 8, respectively), indicating possible changes in the mutual orientation of these α-helices upon binding to eIF4A-NTD. In contrast, eIF4A-CTD binding affected a smaller surface (colored light blue in **Figure 3C**) on eIF4G HEAT-2, adjacent to the eIF4A-NTD binding surface: the loop between helices 1 and 2 and the N-terminal portion of helix 4.

In order to obtain quantitative results about the affinities of the eIF4G HEAT-2:eIF4A domain interactions, we used Surface Plasmon Resonance (SPR). In all SPR experiments in this work, the eIF4G HEAT domains were immobilized on the chip and full-length eIF4A, or eIF4A domains were injected at increasing concentrations. The measured response units (RU) are proportional to the amount of protein bound to the chip. The

equilibrium dissociation constant (K_D) was calculated from the steady state binding at a series of concentrations spanning the range from below to above the K_D of binding, as shown on **Figure 2**.

Consistent with the NMR data, the K_D for the HEAT-2:eIF4A-NTD interaction calculated from SPR binding studies (**Figure S1**, panel **C**) was 70 μM, whereas the HEAT-2:eIF4A-CTD binding was too weak to quantitate by SPR (data not shown).

To characterize further the interactions between eIF4G HEAT-2 and eIF4A, we tested two point mutations in eIF4G HEAT-2 for their effect on eIF4A binding. The D1259N mutation, located in the loop between helices 1 and 2, had previously been reported to affect binding of eIF4G to eIF4A (Yang et al., 2004) and lies within the contact surface of eIF4G HEAT-2 with eIF4A-CTD (see **Figure 3C**). The second mutation, I1293K at the N-terminus of helix 4, has not been studied previously and was selected to lie between the eIF4A-NTD and eIF4A-CTD contact surfaces. I1293 served as a negative control since it is at the periphery of the binding interfaces and it is not expected to affect the interaction of eIF4G HEAT-2 with either eIF4A-CTD or eIF4A-NTD. HSQC spectra (**Figure S1A**) showed that both mutants were folded, with no long-range conformational changes: the only observed effects were in residues in the close vicinity of the mutations. As expected, the D1259N mutation weakened the interaction between eIF4G HEAT-2 and eIF4A-CTD, as observed by NMR titration (see the insets on the right of **Figure S1A**). Consistent with the NMR data, SPR showed that whereas the D1259N mutation affected binding of eIF4G HEAT-2 to full-length eIF4A (**Figure S1B**), it had no effect on binding to eIF4A-NTD (**Figure S1C**). In contrast, the I1293K mutation had little effect on the interactions of eIF4G HEAT-2 with eIF4A.

Residue L1270 at the C-terminus of helix 2, where a mutation was also reported to affect eIF4A binding (Yang et al., 2004), was not affected by either eIF4A-NTD or eIF4A-CTD binding (**Figure 3C**). L1270 is on the opposite surface of eIF4G HEAT-2 **(Figure 1D)** and is buried inside the domain. Therefore, the effect of the mutation on eIF4A binding is likely indirect and mediated by defects in the structure or stability of the domain.

The C-terminal region of eIF4H is sufficient for binding to eIF4A-CTD

NMR chemical shift perturbation assays showed that eIF4H binds to eIF4A-CTD (**Figure S3B**), whereas no obvious binding was observed between eIF4H and eIF4A-NTD (data not shown). The interaction between eIF4A-CTD and eIF4H was relatively weak, in fast exchange on the NMR time scale. To delineate more precisely the eIF4A-binding region of eIF4H, we used two C-terminal fragments: eIF4H-CT-short (the last 47 residues of eIF4H, previously shown to be required for eIF4A binding (Feng et al., 2005)) and eIF4H-CT-long (the last 72 residues of eIF4H). The latter fragment was selected to correspond to the entire region of eIF4H that does not have a counterpart in its homolog CBP20 (**Figure 1B**). The rationale for the longer eIF4H C-terminal construct was that since it corresponds to a region present in eIF4H, but not in CBP20, it could represent an independent structural/functional unit. The majority of the peaks in the spectrum of eIF4H-CT-long (blue contours in **Figure S3A**) overlap with a subset of the peaks in the full-length eIF4H spectrum (black contours). Furthermore, a number of peaks in the HSQC spectrum of eIF4H-CT-long (and the corresponding peaks in the spectrum of full-length eIF4H) are broadened, indicative of conformational exchange.

Therefore, it appears that eIF4H-CT-long is at least partially folded and that its conformation is similar when it is part of full-length eIF4H. In contrast, many of the peaks in the spectrum of eIF4H-CT-short (red contours in **Figure S3A**) do not match peaks in either eIF4H-CT-long or full-length eIF4H.

NMR titration of ^{15}N-labeled eIF4H-CT-long with unlabeled eIF4A-CTD (**Figure S3C**) shows that eIF4H-CT-long binds eIF4A-CTD as well as full-length eIF4H does (**Figure S3B**). Thus, the C-terminal portion of eIF4H is sufficient for eIF4A-CTD binding. It should be noted that eIF4A-CTD binding induced modest chemical shift changes in several peaks corresponding to the N-terminal portion of eIF4H (compare panels **B** and **C** of **Figure S3**). Therefore, eIF4A appears to also contact the RRM domain of eIF4H, at least transiently. Surprisingly, eIF4H-CT-short was also able to bind eIF4A-CTD (**Figure S3D**), even though it appeared to be unfolded and to contain only a subset of the residues affected by eIF4A binding (compare panels **B** and **D** of **Figure S3**).

eIF4A and eIF4H form a stable complex in the presence of ATP

The results shown in **Figure 5C** indicate that ATP, but not ADP, promotes a stable complex between eIF4A and eIF4H. However, it was theoretically possible that the slowly accumulating stable eIF4A:eIF4H complex in the presence of ATP was formed by a one-step binding of a minor species present at low concentration in the eIF4A:ATP sample. If this were the case, one would expect that the slope of the slow-binding curve would increase linearly with increasing the eIF4A concentration. However, binding of eIF4A to eIF4H at several different eIF4A concentrations in the presence of ATP showed that the rate of formation of the stable complex increased with increasing eIF4A

concentration faster than expected from a linear dependence (**Figure S2E**). Such cooperative behavior indicates that the interaction between eIF4A and eIF4H in the presence of ATP is more complex than simple one-step binding. ATP did not significantly stimulate the binding of eIF4H to eIF4A-CTD (data not shown). Therefore, in the presence of nucleotide, eIF4H binds more tightly to full-length eIF4A than to eIF4A-CTD.

eIF4A and eIF4H form a stable ternary complex with eIF4G in the presence of ATP

We used size-exclusion chromatography on mixtures of eIF4A, eIF4H, and eIF4G to explore whether these proteins form a stable ternary complex (**Figure S4**). The eIF4G construct used, called here eIF4G-Se, corresponds to the C-terminal two-thirds of eIF4G and contains all known eIF4A-binding sites (see **Figure 1C**). We first confirmed our observation of a binary complex between eIF4A and eIF4H in the presence of ATP (**Figure 5C** and pink line in **Figure S4A**), noting in the SDS-PAGE analysis of fractions from the separation that the proteins in the mixture elute earlier, starting in fraction 14, than they do individually, starting in fraction 17 (data not shown).

When the three proteins are analyzed together, but ATP is omitted from the running buffer, we observe a complex of eIF4A and eIF4G-Se, eluting together beginning in fraction 9, but eIF4H elutes later, in fraction 15 (**Figure S4C**). Including ATP in the running buffer brings eIF4H into the ternary complex with eIF4A and eIF4G-Se, as it elutes in fraction 12, earlier than when it is in complex with only eIF4A (**Figure S4D**), as expected from the results shown in **Figure 5C**, that ATP significantly stabilizes the association of 4A with 4H.

Supplemental Experimental Procedures

Vectors, protein expression and purification

Throughout this work, we used the human eIF4A1 (406 residues), eIF4G1 (1600 residues), and eIF4H isoform 2 (228 residues) or subcloned fragments thereof. The following constructs were used in this study: eIF4G HEAT-1 (residues 747-993); eIF4G HEAT-1 F978A; eIF4G-CY (residues 994-1138); eIF4G HEAT-2 (residues 1220-1437); eIF4G HEAT-2 D1259N; eIF4G HEAT-2 I1293K; eIF4G-SY (residues 682-1138); eIF4G-Se (residues 682-1600); full-length eIF4A (residues 1-406); eIF4A-NTD (residues 1-239); eIF4A-CTD (residues 237-406); full-length eIF4H (residues 1-228); eIF4H-CT long (residues 157-228); and eIF4H-CT short (residues 182-228). The expression constructs for human eIF4A and eIF4A-CTD were described in (Oberer et al., 2005). The clone expressing eIF4A-NTD was a derivative of pETDuet (Novagen) and has an N-terminal His-tag, followed by a TEV cleavage site. All other proteins and protein fragments used in this study were obtained by PCR cloning into a pENTR-D entry vector using a TOPO cloning kit (Invitrogen). N-terminal His_7 tag, followed by a TEV protease cleavage site were introduced with the PCR primers. The constructs were transferred from the entry vector into a Gateway destination vector in frame with an N-terminal GB1 tag, under the control of a T7 promoter, using a Gateway LR Clonase kit (Invitrogen). The resulting expression vectors had an N-terminal GB1 tag for improved expression and solubility (Zhou et al., 2001), followed by an internal His_7 tag and a TEV protease cleavage site. Point mutations and in-frame stop codons were introduced using a QuikChange mutagenesis kit (Stratagene). Expression and purification of unlabeled

proteins, as well as of proteins uniformly labeled with stable isotopes for the NMR experiments, was carried out as previously described for eIF4A-CTD (Oberer et al., 2005).

NMR resonance assignments and chemical shift perturbation assay

NMR spectra were recorded at 298 K on a Bruker 750, 600, or 500 MHz, or a Varian Inova 600 or 500 MHz spectrometers, equipped with cryogenic probes. Unless stated otherwise, samples for NMR measurements contained 0.4–1 mM protein in buffer containing 20 mM Tris-HCl (pH 7.0), 150 mM KCl, 2 mM DTT, 1 mM EDTA, 0.01% NaN_3, 0.2 mM AEBSF, and 10% D_2O. The samples of eIF4A-CTD were at 150 μM or lower, due to the limited solubility of these proteins at physiological salt concentrations.

Backbone resonance assignments were obtained on a 1 mM sample of [^{2}H,^{15}N,^{13}C] eIF4G-HEAT2 in buffer containing 10% D_2O, 20 mM Tris pH 7.0, 150 mM NaCl, 0.5 mM EDTA, 2 mM DTT, using the following triple-resonance experiments: HNCA, HN(CO)CA, HN(CA)CB, HN(COCA)CB, HNCO, and HN(CA)CO. The spectra were processed with NMRPipe (Delaglio et al., 1995) and analyzed with CARA (Keller, 2004). Backbone resonance assignments were obtained for 100 % of the assignable residues in the eIF4G HEAT-2 domain.

Chemical shift mapping was done as described in (Marintchev et al., 2007). Briefly, one of the interacting proteins was uniformly ^{15}N-labeled. ^{15}N-HSQC or TROSY-HSQC spectra were collected for the free protein and in the presence of increasing concentrations of the unlabeled protein until all the labeled protein was bound, unless limited by solubility.

Surface Plasmon Resonance (SPR)

SPR experiments were carried out using a BIAcore 3000 instrument (Biacore Inc., Piscataway, NJ). Wild-type or mutant eIF4G HEAT-1, eIF4G HEAT-2, or eIF4H were immobilized on a research grade CM5 sensor chip using amino coupling kit in 10 mM sodium acetate, pH 5.5. A control flowcell was subjected to activation and blocking following the same protocol but without proteins. The surface densities of immobilized proteins were between 2000 and 3000 Response Unit (RU). The binding experiments were carried out in the buffer described above for the NMR experiments at 25^{o}C, at flow rate of 20 μl/min. eIF4A, eIF4A-NTD, or eIF4A-CTD was injected at increasing concentrations. 1 mM ATP (or ADP) and 3 mM $MgCl_2$ was added to the injected eIF4A samples, where indicated. The signal generated in the control flowcell was subtracted from the experimental signals to correct for refractive index changes and nonspecific binding. To rule out mass transfer effects, control experiments were performed at various flow rates, as recommended by the manufacturer. Curve fitting was done with SigmaPlot (SPSS Inc.).

In the SPR experiments, if the binding is tight (K_D in the nanomolar range), the binding partner is injected at low concentration, comparable to the K_D, and gradual signal build-up is observed. At the end of the injection, gradual loss of signal is observed as the bound protein is slowly released. The build-up and release curves can be used to fit the rate constants k_{on} and k_{off}, and the K_D. If the binding is weaker (K_D in the micromolar range), higher concentrations of protein need to be injected to see binding, leading to steep build-up curves; and the steady state equilibrium between binding and release is

reached almost instantaneously. For weak interactions, the k_{off} is usually very fast and therefore the release at the end of the injection is also almost instantaneous. Whereas rate constants cannot be fit for such weak interactions, the K_D can be calculated by plotting the steady state equilibrium binding as a function of the concentration of the injected species.

Fluorescence Anisotropy

Fluorescence anisotropy RNA binding experiments were carried out in 384-well plates on a PerkinElmer EnVision plate reader. The samples contained 50 nM FITC-labeled U_{40} RNA oligonucleotide (Dharmacon). When the fluorophore (FITC) is excited with polarized light, the degree of retention of polarization/anisotropy of the emitted light depends on the tumbling rate of the fluorophore. Protein binding to the RNA oligonucleotide results in formation of larger complexes with slower tumbling rates, which is detected as increase in polarization (anisotropy). The binding experiments were carried out in the buffer described above for the NMR experiments at 25°C, in the presence of 5 mM $MgCl_2$, and 20 units/ml RNase inhibitor (Invitrogen). Curve fitting was done with SigmaPlot (SPSS Inc.), as described in (Roehrl et al., 2004) for direct binding.

For the competition experiments shown in **Figure 6B**, it was not possible to distinguish unambiguously whether the binding of eIF4G HEAT-2 and RNA to eIF4A was purely competitive (no RNA binding to eIF4A at saturating concentrations of HEAT-2) or the HEAT-2:eIF4A complex retained weak residual affinity for RNA. Therefore, the results from the competition experiments were fit to an equation for incomplete

competitive binding. The general treatment of incomplete competitive binding yields a fifth-degree polynomial (Roehrl et al., 2004). However, the concentration of the FITC-labeled RNA oligonucleotide (50 nM) was negligible compared to the protein concentrations used, and RNA binding did not affect the concentration of the free proteins and protein:protein complexes, which simplified the equation significantly compared to the general case, described in (Roehrl et al., 2004).

Isothermal Titration Calorimetry (ITC)

ITC binding experiments were carried out on a VP-ITC machine (MicroCal). Titrations were performed at 25°C by injecting 30 consecutive aliquots of 10 µl of eIF4G HEAT-2 (135 µM - 328 µM) into a 1.4 ml well containing eIF4A (15 µM - 36 µM) with and without eIF4G HEAT-1 (50 µM), in a buffer containing 20 mM Tris pH 7.0, 150 mM NaCl, 0.5mM EDTA, 5 mM $MgCl_2$, 2 mM TCEP, and 5% glycerol. Data were processed using Origin software.

Analytical size-exclusion chromatography

Analytical size exclusion chromatography was performed on an analytical Superdex 200 (GE Healthcare) column, with running buffer containing 20 mM Tris (pH 7.0), 150 mM NaCl, 2 mM DTT, 5% glycerol, 5 mM $MgCl_2$, and 0.5 mM EDTA. Except where indicated otherwise, the buffer also included 1 mM ATP. Injected samples contained each indicated protein at a 10 µM concentration, along with 10 µM FITC-U_{40} and 1 mM AMPPNP. 0.5 ml fractions were collected beginning at 7 minutes after injection, and analyzed by SDS-PAGE.

Structure analysis and modeling

The interdomain orientation between eIF4A-NTD, eIF4A-CTD, and the RNA were modeled based on the structure of eIF4A-III within the Exon Junction Complex (PDB code 2HYI, (Andersen et al., 2006)). For modeling, we used the crystal structure of human eIF4A-NTD (PDB code 2G9N) and a homology model for eIF4A-CTD, based on the structure of yeast eIF4A, which is described elsewhere (Oberer et al., 2005). Sequence homology analysis and alignments were done using PSI-BLAST (Altschul et al., 1997), CLUSTAL-W (Thompson et al., 1994), and T-COFFEE (Notredame et al., 2000). Structure analysis, comparisons and alignments were performed using MOLMOL (Koradi et al., 1996) and Dali (Holm and Sander, 1993). Homology modeling was done using SWISS-MODEL (Arnold et al., 2006). The interdomain orientation of the HEAT domains of eIF4G was as modeled previously (Marintchev and Wagner, 2005), based on the interdomain orientation in CBP80 in the nuclear Cap-binding complex (PDB code 1HT2 (Mazza et al., 2002)). The topology of the eIF4A/4G/4H complex was built interactively in MOLMOL, guided by the results from NMR chemical shift mapping and site-directed mutagenesis. Modeling of the position of the eIF4A/4G/4H complex on the ribosome was done in MOLMOL, which was also used to generate the resulting figures.

Supplemental References

Altschul, S.F., Madden, T.L., Schaffer, A.A., Zhang, J., Zhang, Z., Miller, W., and Lipman, D.J. (1997). Gapped BLAST and PSI-BLAST: a new generation of protein database search programs. Nucleic Acids Res *25*, 3389-3402.

Andersen, C.B., Ballut, L., Johansen, J.S., Chamieh, H., Nielsen, K.H., Oliveira, C.L., Pedersen, J.S., Seraphin, B., Le Hir, H., and Andersen, G.R. (2006). Structure of the exon

junction core complex with a trapped DEAD-box ATPase bound to RNA. Science *313*, 1968-1972.
Arnold, K., Bordoli, L., Kopp, J., and Schwede, T. (2006). The SWISS-MODEL workspace: a web-based environment for protein structure homology modelling. Bioinformatics *22*, 195-201.
Delaglio, F., Grzesiek, S., Vuister, G.W., Zhu, G., Pfeifer, J., and Bax, A. (1995). NMRPipe a Multidimensional Spectra Processing System Based on UNIX Pipes. JBNMR *6*, 277-293.
Feng, P., Everly, D.N., Jr., and Read, G.S. (2005). mRNA decay during herpes simplex virus (HSV) infections: protein-protein interactions involving the HSV virion host shutoff protein and translation factors eIF4H and eIF4A. J Virol *79*, 9651-9664.
Holm, L., and Sander, C. (1993). Protein structure comparison by alignment of distance matrices. J Mol Biol *233*, 123-138.
Keller, R.L.J. (2004). The Computer Aided Resonance Assignment Tutorial (Goldau, Cantina Verlag).
Koradi, R., Billeter, M., and Wuthrich, K. (1996). MOLMOL: a program for display and analysis of macromolecular structures. J Mol Graph *14*, 51-55, 29-32.
Marcotrigiano, J., Lomakin, I.B., Sonenberg, N., Pestova, T.V., Hellen, C.U., and Burley, S.K. (2001). A conserved HEAT domain within eIF4G directs assembly of the translation initiation machinery. Mol Cell *7*, 193-203.
Marintchev, A., Frueh, D., and Wagner, G. (2007). NMR methods for studying protein-protein interactions involved in translation initiation. Methods Enzymol *430*, 283-331.
Marintchev, A., and Wagner, G. (2005). eIF4G and CBP80 share a common origin and similar domain organization: implications for the structure and function of eIF4G. Biochemistry *44*, 12265-12272.
Mazza, C., Segref, A., Mattaj, I.W., and Cusack, S. (2002). Large-scale induced fit recognition of an m(7)GpppG cap analogue by the human nuclear cap-binding complex. EMBO J *21*, 5548-5557.
Notredame, C., Higgins, D.G., and Heringa, J. (2000). T-Coffee: A novel method for fast and accurate multiple sequence alignment. J Mol Biol *302*, 205-217.
Oberer, M., Marintchev, A., and Wagner, G. (2005). Structural basis for the enhancement of eIF4A helicase activity by eIF4G. Genes Dev *19*, 2212-2223.
Roehrl, M.H., Wang, J.Y., and Wagner, G. (2004). A general framework for development and data analysis of competitive high-throughput screens for small-molecule inhibitors of protein-protein interactions by fluorescence polarization. Biochemistry *43*, 16056-16066.
Thompson, J.D., Higgins, D.G., and Gibson, T.J. (1994). CLUSTAL W: improving the sensitivity of progressive multiple sequence alignment through sequence weighting, position-specific gap penalties and weight matrix choice. Nucleic Acids Res *22*, 4673-4680.
Yang, H.S., Cho, M.H., Zakowicz, H., Hegamyer, G., Sonenberg, N., and Colburn, N.H. (2004). A novel function of the MA-3 domains in transformation and translation suppressor Pdcd4 is essential for its binding to eukaryotic translation initiation factor 4A. Mol Cell Biol *24*, 3894-3906.
Zhou, P., Lugovskoy, A.A., and Wagner, G. (2001). A solubility-enhancement tag (SET) for NMR studies of poorly behaving proteins. J Biomol NMR *20*, 11-14.

Figure S1.

Effects of mutations in eIF4G HEAT-2 at and near the eIF4A-CTD contact surface

A. Overlay of the ^{15}N HSQC spectra of GB1 fusions of the WT eIF4G HEAT-2 domain (black), HEAT-2 I1293K (cyan), and HEAT-2 D1259N (orange). Insets on the right: **1.** (top) A zoomed-in region of the spectra on the left. **2.** The corresponding region from the overlay of the spectra of WT HEAT-2 in the presence (red) and absence (black) of eIF4A-CTD from Fig. 3B. **3.** The corresponding region from the overlay of the spectra of HEAT-2 I1293K in the presence (red) and absence (black) of eIF4A-CTD. **4.** The corresponding region from the overlay of the spectra of HEAT-2 D1259N in the presence (red) and absence (black) of eIF4A-CTD. "+" designates binding between HEAT-2 and eIF4A-CTD; "+/-" for HEAT-2 D1295N designates binding that appears weaker than that of the WT HEAT-2 domain.

B. The D1259N mutation in eIF4G HEAT-2 affects binding to eIF4A, but not to eIF4A-NTD. SPR binding curves of immobilized WT eIF4G HEAT-2 (black), HEAT-2 I1293K (blue), and HEAT-2 D1259N (red) with full-length eIF4A. The calculated K_D values are shown next to the graphs.

C. SPR binding curves of immobilized WT eIF4G HEAT-2 (black), HEAT-2 I1293K (blue), and HEAT-2 D1259N (red) with eIF4A-NTD. Note that binding of eIF4A-NTD (panel **C**) gives rise to half the response from the same number of full-length eIF4A molecules (panel **B**), because eIF4A-NTD is 25 kDa, whereas eIF4A is 45 kDa. Curve fitting was done with SigmaPlot (SPSS Inc.).

Figure S2.

eIF4H binding to eIF4A

A. Overlay of ^{15}N HSQC spectra of full-length eIF4H (black), eIF4H-CT-long (cyan), and eIF4H-CT-short (red) proteins. The positions of peaks in eIF4H affected by eIF4A-CTD binding (see panel **B**) are marked with an orange cross: most but not all of these peaks are present in the spectrum of eIF4H-CT-long, indicating that the C-terminal region of eIF4H is the main eIF4A-CTD binding site.

B. ^{15}N HSQC spectrum of eIF4H in the presence (red) and absence (black) of eIF4A-CTD. Peaks affected by eIF4A-CTD binding are marked with an orange cross in the inset on the right (the same region is zoomed-in as in panel **A**).

C. ^{15}N HSQC spectrum of eIF4H-CT-long in the presence (red) and absence (black) of eIF4A-CTD. Only the portion of the spectrum zoomed-in in panel **A** is shown. Both the starting and final positions of most peaks affected by eIF4A-CTD binding are the same as in full-length eIF4H (Panel **B**).

D. ^{15}N HSQC spectrum of eIF4H-CT-short in the presence (red) and absence (black) of eIF4A-CTD. Only the portion of the spectrum zoomed-in in panel **A** is shown.

The position of one of the peaks belonging to residues from the C-terminal region of eIF4H that are affected by eIF4A-CTD binding is circled and marked with "1" in the inset of panel **B** and in panel **C**, as well as in panel **D**, where the peak is missing. The position of one of the peaks belonging to residues from the RRM domain of eIF4H that are weakly affected by eIF4A-CTD binding is circled and marked with "2" in the inset of panel **B** as well as in panels **C** and **D**, where the peak is missing.

E. Overlay of SPR sensorgrams showing binding of eIF4A to immobilized eIF4H in the presence of 1 mM ATP.

Figure S3.

Comparison between the CBP80/CBP20 complex and the eIF4A/4G/4H complex

A. The structure of the CBP80/CBP20 complex (Mazza et al., 2002) in surface representation. The HEAT-1 and HEAT-2 domains of CBP80 are in yellow and orange, respectively. The first four helical hairpins of the CBP80 HEAT-3 domain are in dark orange. The last two helical hairpins (with no counterpart in the eIF4G HEAT-3 domain) are also colored dark orange, but shown semi-transparent, overlaid on the ribbon. The interdomain linkers are in grey. CBP20 is in violet, and the RNA is in red.

B. The topology of the eIF4A/4G/eIF4H complex (as in Fig. 5). The orientation of eIF4A with respect to eIF4G is based on NMR chemical shift mapping (this work and (Oberer et al., 2005)). Domains, whose structures are known or could be modeled, are displayed as solid bodies with size and shape corresponding to their structures, providing a rough model of the size and topology of the complex. The HEAT-1, -2 and -3 domains of eIF4G are in yellow, orange and dark orange, respectively. The eIF4G interdomain linker is not shown. eIF4A-NTD is in blue and eIF4A-CTD is in light blue. The eIF4H-RRM is in violet. eIF4H-CTD, whose structure is not known, is shown as a circle. The mRNA is in red. The orientation in the right panel is obtained by 180º rotation along the Y-axis in the direction of the arrows: thus the left and right panel show opposite surfaces of the complex.

The position of the mRNA on eIF4A is modeled based on the structure of eIF4A-III within the Exon Junction Complex (PDB code 2HYI, (Andersen et al., 2006)). The RNA-binding site of the eIF4H RRM domain is based on that of its homolog CBP20 in the CBP80/CBP20 complex (Mazza et al., 2002). The RNA-binding site of the eIF4G HEAT-1 domain (marked with a star) is based on mutation data (Marcotrigiano et al., 2001).

Figure S4.

Size-exclusion chromatography of eIF4G/4A/4H ternary complex

A. Chromatograms from analytical gel filtration of a mixture of eIF4G-Se, eIF4A, and eIF4H, run with and without ATP in the buffer (blue line and dashed black line, respectively), and of a mixture of eIF4A and eIF4H, run with ATP in the buffer (pink line). Absorption at 280 nm is plotted versus elution time and fraction number for the three mixtures. The eIF4G-Se construct corresponds to the C-terminal two-thirds of eIF4G (see **Figure 1C**).

B. SDS-PAGE analysis of fractions collected from separation of the mixture of eIF4A and eIF4H. The two proteins begin to elute in fraction 14, earlier than they elute when run separately (data not shown), indicating that they form a complex.

C. SDS-PAGE analysis of fractions collected from separation of the eIF4G-Se/eIF4A/eIF4H mixture, without ATP in the running buffer. Bands of eIF4G-Se, eIF4A, and eIF4H are labeled. Remaining bands are degradation products of eIF4G-Se, some of which are marked with asterisks. eIF4A elutes as early as eIF4G-Se, beginning in fraction

9, indicating binary complex formation. In the absence of ATP, eIF4H does not join the complex: it begins to elute only in fraction 15.

D. SDS-PAGE analysis of fractions collected from separation of the eIF4G-Se/eIF4A/eIF4H mixture, with ATP in the running buffer. As in the case without ATP, eIF4A elutes early with eIF4G-Se, indicating complex formation. In this case, however, eIF4H also elutes significantly earlier than it does in the binary eIF4A/4H complex, now beginning in fraction 12.

Supplemental Figure 1

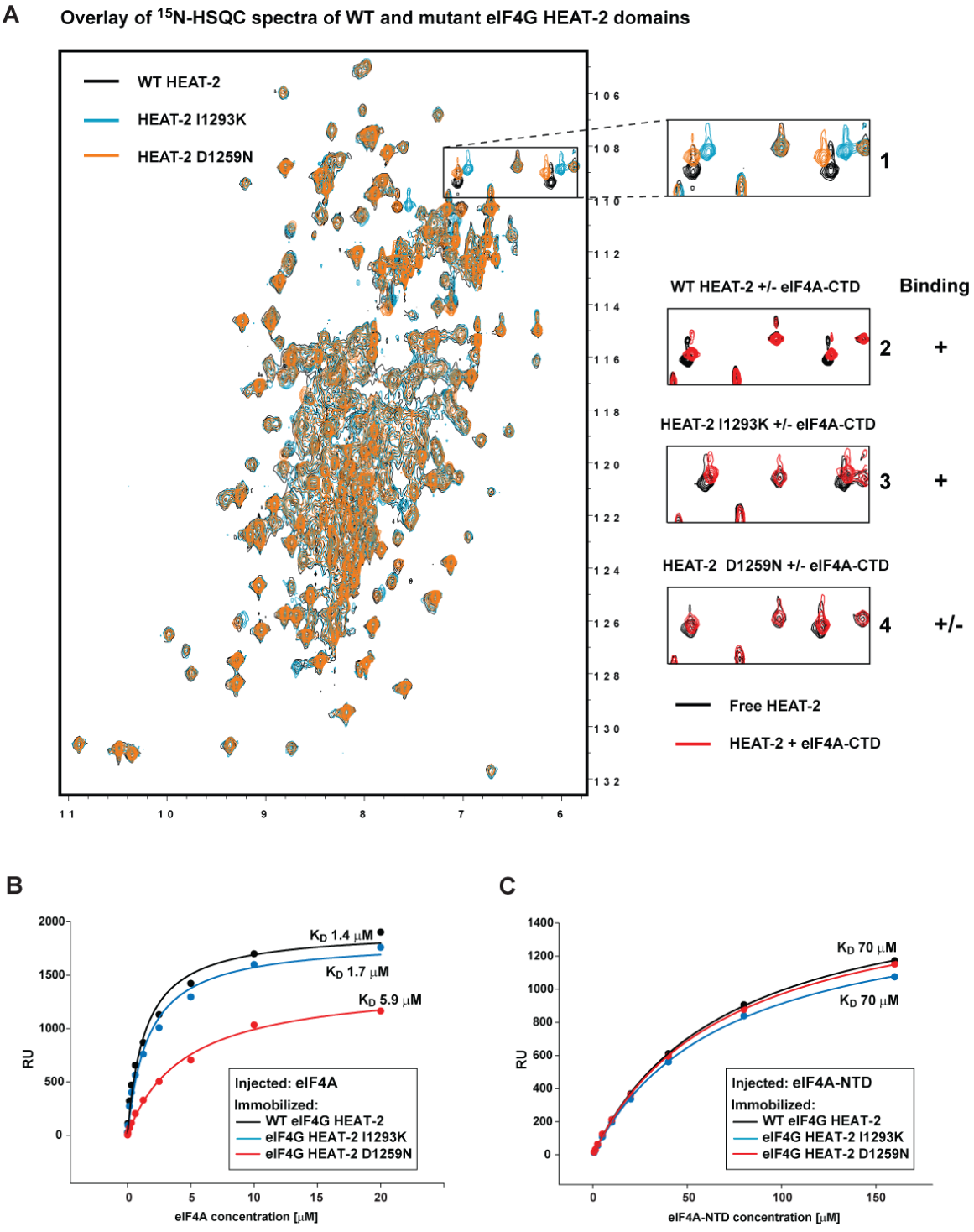

Supplemental Figure 2

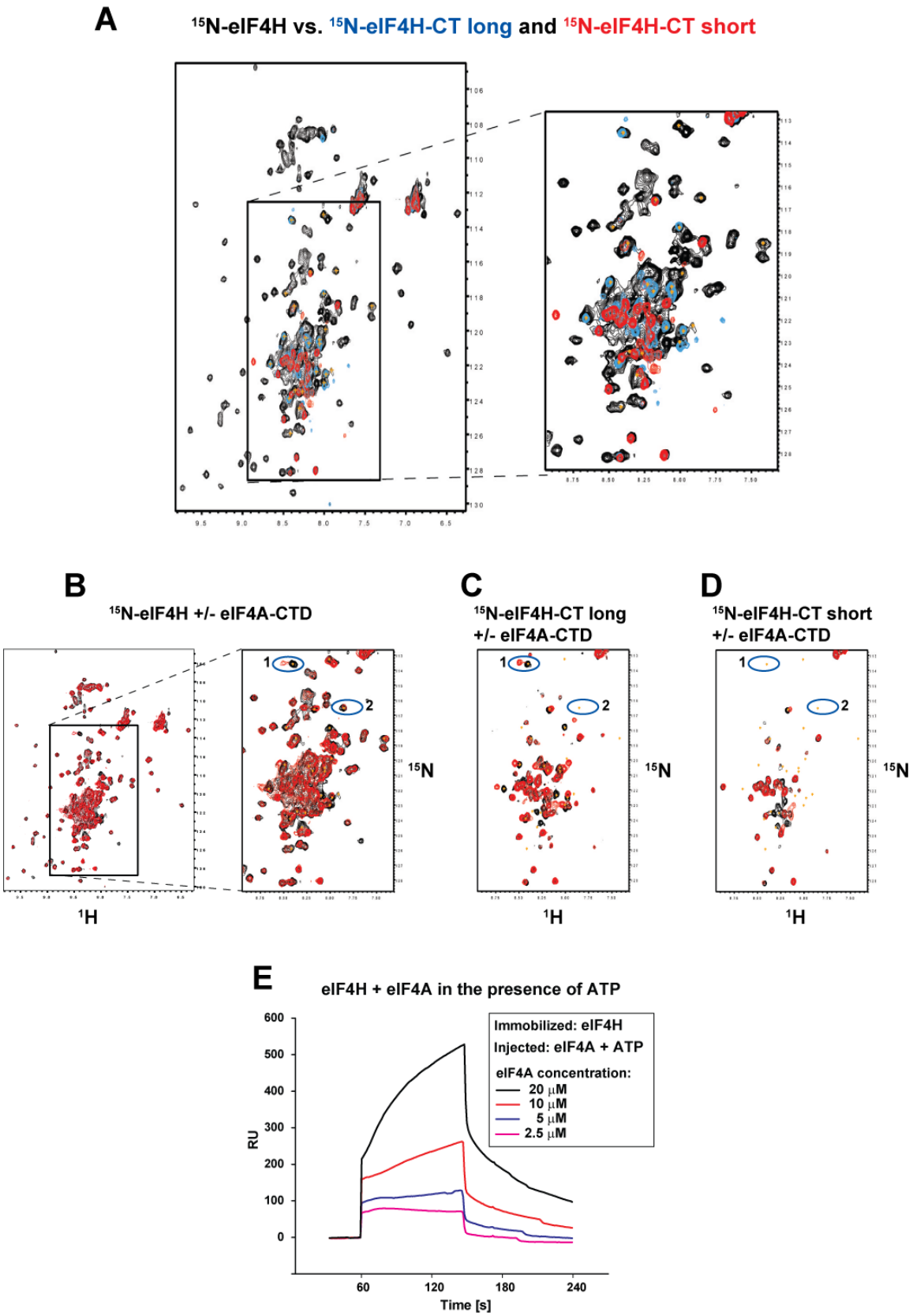

Supplemental Figure 3

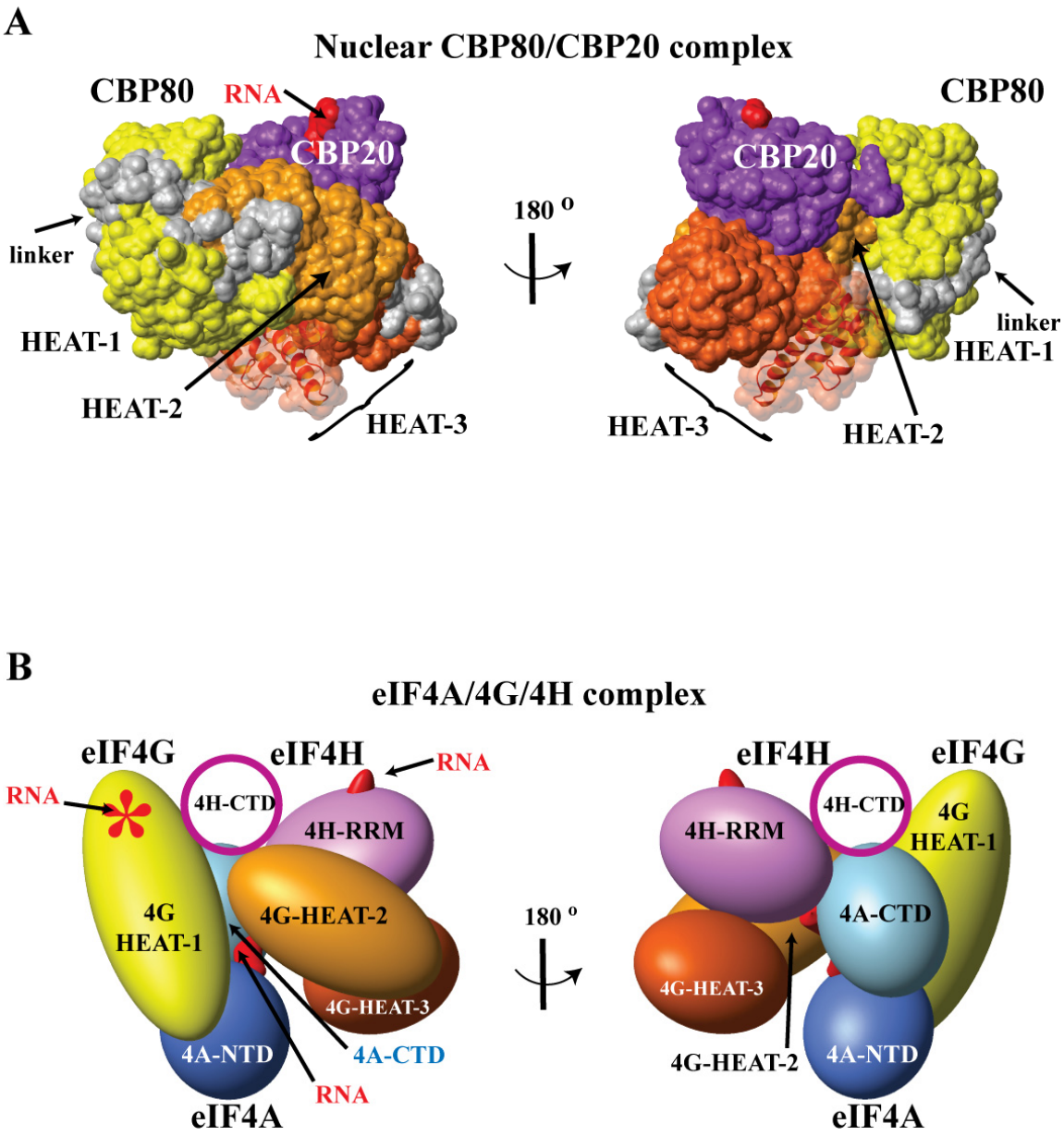

Supplemental Figure 4

A. Size-exclusion chromatography of eIF4G/4A/4H mixtures

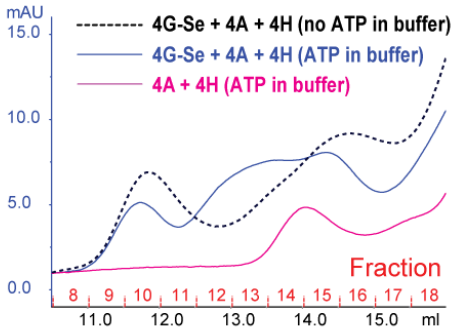

B. SDS-PAGE of fractions shows that eIF4H co-migrates with eIF4A

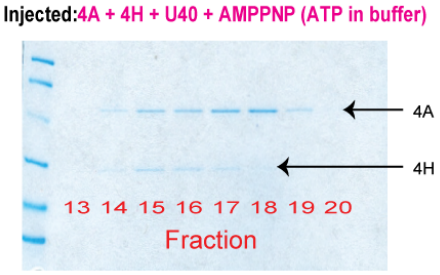

C. eIF4H does not co-migrate with eIF4G-Se and eIF4A when ATP is omitted

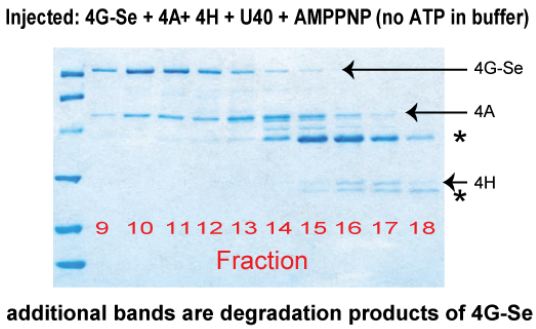

* additional bands are degradation products of 4G-Se

D. eIF4H co-migrates with eIF4G-Se and eIF4A in the presence of ATP